

CAR T cell infiltration and cytotoxic killing within the core of 3D breast cancer spheroids under the control of antigen sensing in microwell arrays

Cite as: APL Bioeng. **8**, 036105 (2024); doi: 10.1063/5.0207941

Submitted: 12 March 2024 · Accepted: 3 July 2024 ·

Published Online: 23 July 2024



View Online



Export Citation



CrossMark

Youngbin Cho,¹  Matthew S. Laird,¹  Teddi Bishop,¹  Ruxuan Li,¹  Dorota E. Jazwinska,¹  Elisa Ruffo,^{2,3} 
Jason Lohmueller,^{2,3}  and Ioannis K. Zervantonakis^{1,2,a)} 

AFFILIATIONS

¹Department of Bioengineering, University of Pittsburgh, Pittsburgh, Pennsylvania 15219, USA

²Hillman Cancer Center, University of Pittsburgh, Pittsburgh, Pennsylvania 15232, USA

³Department of Surgery, Division of Surgical Oncology, University of Pittsburgh, Pittsburgh 15213, Pennsylvania, USA

Note: This paper is part of the special issue on Physical Sciences Approaches to Cancer Research.

^{a)}Author to whom correspondence should be addressed: ioz1@pitt.edu

ABSTRACT

The success of chimeric antigen receptor (CAR) T cells in blood cancers has intensified efforts to develop CAR T therapies for solid cancers. In the solid tumor microenvironment, CAR T cell trafficking and suppression of cytotoxic killing represent limiting factors for therapeutic efficacy. Here, we present a microwell platform to study CAR T cell interactions with 3D breast tumor spheroids and determine predictors of anti-tumor CAR T cell function. To precisely control antigen sensing, we utilized a switchable adaptor CAR system that covalently attaches to co-administered antibody adaptors and mediates antigen recognition. Following the addition of an anti-HER2 adaptor antibody, primary human CAR T cells exhibited higher infiltration, clustering, and secretion of effector cytokines. By tracking CAR T cell killing in individual spheroids, we showed the suppressive effects of spheroid size and identified the initial CAR T cell to spheroid area ratio as a predictor of cytotoxicity. We demonstrate that larger spheroids exhibit higher hypoxia levels and are infiltrated by CAR T cells with a suppressed activation state, characterized by reduced expression of IFN- γ , TNF- α , and granzyme B. Spatiotemporal analysis revealed lower CAR T cell numbers and cytotoxicity in the spheroid core compared to the periphery. Finally, increasing CAR T cell seeding density resulted in higher CAR T cell infiltration and cancer cell elimination in the spheroid core. Our findings provide new quantitative insight into CAR T cell function within 3D cancer spheroids. Given its miniaturized nature and live imaging capabilities, our microfabricated system holds promise for screening cellular immunotherapies.

© 2024 Author(s). All article content, except where otherwise noted, is licensed under a Creative Commons Attribution-NonCommercial 4.0 International (CC BY-NC) license (<https://creativecommons.org/licenses/by-nc/4.0/>). <https://doi.org/10.1063/5.0207941>

INTRODUCTION

Chimeric antigen receptors (CARs) have emerged as a promising approach to develop cell-based immunotherapies.^{1–3} CARs, composed of an antigen-specific antibody single chain variable fragment fused to T cell signaling domains, have been used to engineer T cells that are activated upon binding to a target antigen. CAR T cell-based immunotherapies have been FDA-approved for acute lymphoblastic leukemia and multiple myeloma.^{4–7} Developing CAR T cells that recognize targets enriched in solid tumors, such as human epidermal growth factor receptor 2 (HER2), has been a major research focus, yet the clinical trials have not been successful to date.^{7,8} The antitumor function of CAR T cells in solid tumors relies on efficient trafficking within the tumor

microenvironment and sustained cytotoxic activity.^{9–12} Since these processes involve dynamic cell–cell interactions, a comprehensive profiling of tumor–CAR T cell crosstalk and antigen-specific cytotoxicity is crucial to understanding mechanisms that enhance CAR T cell therapeutic efficacy.

Preclinical testing of CAR T cell cytotoxicity *in vivo* has provided valuable insight into identifying potent CAR T cell therapies,^{13,14} however, these models are costly and pose challenges for investigating dynamic cell–cell interactions. While intravital imaging allows for monitoring immune cell trafficking and cytotoxicity, its duration is limited to a few hours, and the control of the tumor microenvironment is challenging.^{15,16} Several *in vitro* studies have employed cocultures of

CAR T cells with tumor cells to measure CAR T cell function by colorimetric cytotoxicity assays.^{17–21} While these assays offered a rapid and straightforward evaluation of CAR T cell function, they typically provide a single time-point measurement. Assays using micropatterning of tumor cell islands allowed for spatial segregation of each cell type and are compatible with time-lapse imaging.²² However, as the tumor cells were plated on a two-dimensional surface, it is challenging to recreate the three-dimensional architecture of the solid tumor microenvironment.

Spheroids serve as more physiologically relevant 3D *in vitro* models, allowing assessment of drug sensitivity,^{23–26} hypoxic gradients,²⁷ and tumor-immune cell signaling.^{28–30} To model CAR T cell–cancer spheroid interactions, previous studies have used ultra-low adhesion well plates^{17,31} or hanging drop assays.^{32–34} These methods are simple, requiring no special equipment, but they are labor-intensive and pose challenges in obtaining high-resolution images for the dynamic profiling of cell–cell interactions.^{35,36} Microfabrication technologies present a promising approach to control and monitor T cell interactions with cancer spheroids. For example, microfluidic devices seeded with T cell receptor-engineered T cells and cancer spheroids revealed differences in T cell migratory behavior and cytotoxic efficiency between 2D and 3D *in vitro* environments.³⁷ Another microfluidic study demonstrated how enhanced vascularization of cancer spheroids is critical for CAR T cell delivery and cytotoxic function.³⁸ Furthermore, a microfluidic platform has previously shown the generation of cancer spheroids with co-encapsulation of stromal cells to test combination immunotherapies with CAR T cells.³⁹ Despite these advances, the spatiotemporal patterns of CAR T cell infiltration and cytotoxicity following sensing of a target antigen, as well as the effects of different spheroid sizes on CAR T cell anti-tumor function remain poorly understood.

In this study, we developed a microwell-based assay to monitor the dynamic processes of CAR T cell infiltration and cytotoxicity in 3D cancer spheroids. To evaluate the antigen-specific antitumor activity of CAR T cells, we utilized a switchable adaptor CAR system, SNAP-CAR, which mediates tumor antigen recognition through the covalent attachment of a co-administered antibody adaptor bearing a benzylguanine motif.⁴⁰ This adaptor system allows for universal targeting of antigens and functional profiling within the same batch of engineered CAR T cells.^{41–51} Specifically, we assessed CAR T cell cytotoxicity against HER2+ breast cancer spheroids in the presence or absence of an adaptor antibody that recognizes the HER2 antigen, Herceptin.⁵² Through the fabrication of thin polydimethylsiloxane-based microwells using spin coating, we were able to perform high-resolution, live confocal imaging. Our microwell array facilitated monitoring of CAR T cell clustering and cytotoxicity in individual spheroids over time and led to the identification of the initial CAR T cell to spheroid area ratio as a predictor of cytotoxicity efficiency. Using a range of spheroid sizes and effector to target ratios, we demonstrated the suppressive mechanism of larger spheroids on CAR T cell cytotoxicity, activation state, and secretion of effector cytokines and proteases. Additionally, the spatiotemporal analysis of CAR T cell functions demonstrated distinct patterns of CAR T cell-mediated killing in the spheroid core compared to the periphery. These results demonstrate the utility of the microwell array platform for elucidating dynamic interactions of CAR T cells with 3D cancer spheroids following antigen sensing that promotes CAR T cell clustering and elimination of HER2+ breast cancer cells. Finally, our studies on CAR T cell

function within the spheroid core have important implications for the design of cell-based immunotherapies to promote immune cell trafficking in solid tumors.

RESULTS

Formation of 3D spheroids using HER2+ breast cancer cells in microwell arrays

We developed an array of microwells with controllable size to form 3D cancer spheroids under conditions that allowed high-resolution imaging. Microwells were fabricated using polydimethylsiloxane (PDMS) patterned onto an SU-8 silicon wafer using spin coating to create devices with $\sim 270\ \mu\text{m}$ thickness that are compatible with high numerical aperture objectives [Figs. 1(a) and 1(c)]. The microwells were bonded onto a 24-well glass-bottom plate to enable stable long-term live cell microscopy and minimize the evaporation of the cell culture medium. Coating of microwell surfaces with a pluronic solution prevented cell adhesion and promoted cell–cell clustering under suspension culture. We found that HER2+ breast cancer cell lines BT474 and EFM192A could efficiently form spheroids in our microwell array [Figs. 1(c) and S1]. As expected, spheroid diameter increased for microwells with larger side lengths [Figs. 1(d) and 1(e) and S1(a) and S1(b)]. We found that microwells with a side length of $50\ \mu\text{m}$ included a spheroid that occupied the whole microwell area [Figs. 1(f) and S1(c)]. Similarly, the majority of the microwell area was occupied with the spheroid for a side length of $100\ \mu\text{m}$. Finally, for microwells with a side length of $200\ \mu\text{m}$, there was greater than 50%–75% free surface area on the microwell, where another cell type could be introduced to monitor dynamic cell–cell interactions [Figs. 1(f) and S1(c)].

CAR T cell sensing of HER2 on cancer cells stimulates cytotoxicity and promotes CAR T cell infiltration within 3D cancer spheroids

To study antigen-specific CAR T cell function, we seeded CAR T cells in the microwells ($200 \times 200\ \mu\text{m}$) with HER2+ breast cancer spheroids that were previously formed [Fig. 2(a)]. We utilized the SNAP-CAR “universal” adaptor CAR system, for which the SNAPtag protein takes the place of the antigen binding region and, instead of directly binding to an antigen on a cancer cell, covalently attaches to a benzylguanine (BG)-conjugated antibody.⁴⁰ Specifically, we tested the HER2-specific antibody adaptor, BG-Herceptin.⁵² This adaptor antibody binds to HER2+ cancer cells via the variable region of the antibody, while the BG motif reacts with the SNAPtag fusing it to the CAR T cells [Fig. 2(b)]. To evaluate the performance of the adaptor-directed CAR T cells, we analyzed the overlap of a dead cell marker [cyan, Fig. 2(c)] with a cancer cell-specific marker [red, Figs. 2(c) and S2]. We found higher cancer cell death for both BT474 spheroids and EFM192A spheroids in the presence of the BG-Herceptin adaptor compared to control cocultures with no adaptor. Specifically, 62% of the cancer spheroid area colocalized with dead cell staining for BT474 spheroids (average value across all spheroids) treated with BG-Herceptin compared to 25% in the untreated control ($p < 0.0001$), and a similar response was observed for EFM192A spheroids with 46% and 17% ($p < 0.0001$), respectively [Figs. 2(d) and S3]. To examine CAR T cell cytotoxicity within a 3D matrix, we embedded BT474 spheroids within a collagen type I matrix and seeded CAR T cells outside the matrix. We found that treatment with BG-Herceptin increased

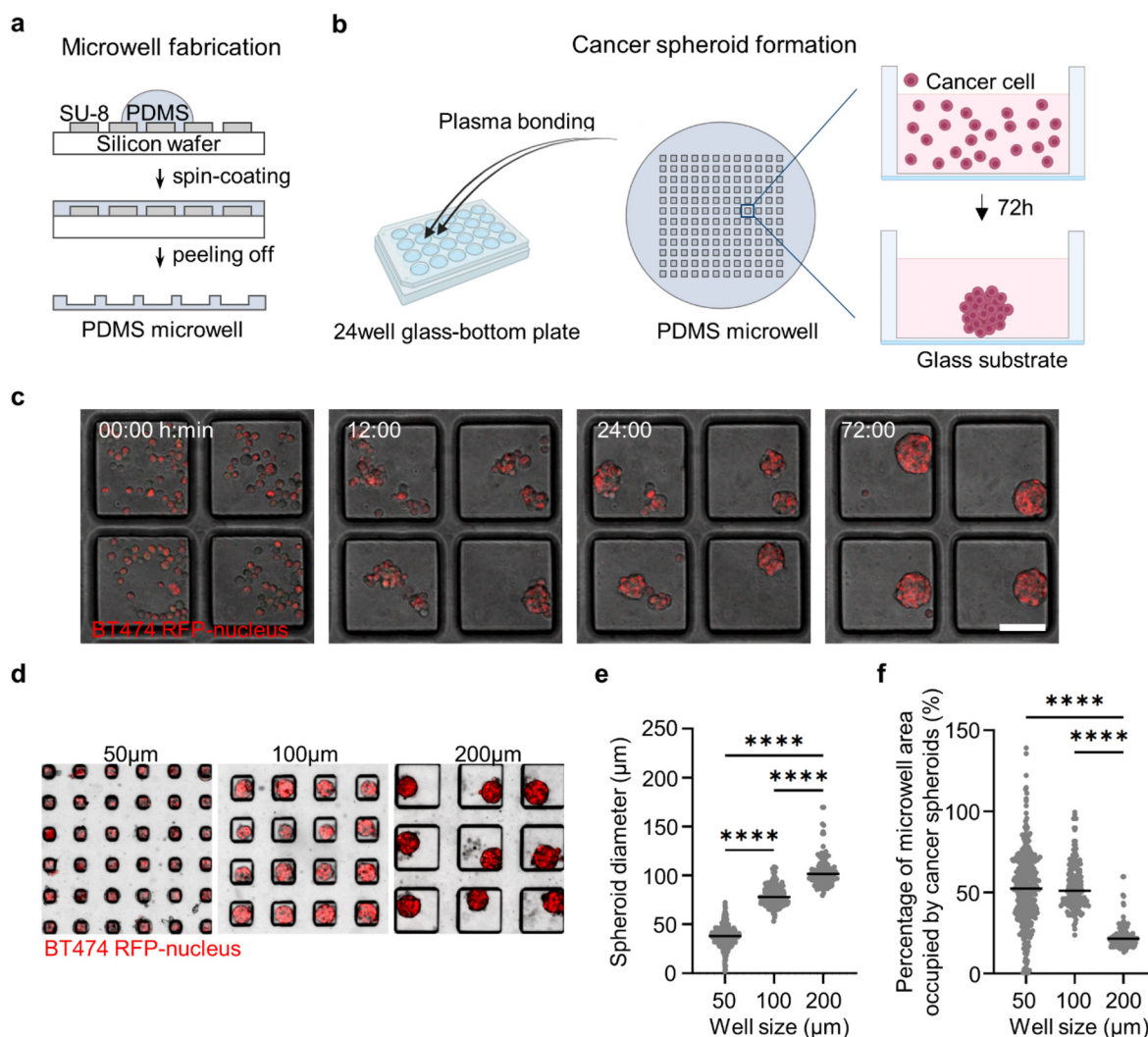


FIG. 1. Microwell array platform to form and immobilize HER2+ breast cancer spheroids. (a) Schematics of PDMS microwell fabrication on SU-8 silicon wafer. (b) Bonding of PDMS microwell array on glass-bottom platform and cell seeding to form cancer spheroids. (c) Time-lapse images showing the spheroid formation of BT474-H2BRFP cells in microwells over 72 h. Scale bars, 100 μm . (d) Spheroid formation of BT474 cells in microwells with varying side length (50, 100, and 200 μm). (e) Quantification of the diameter of BT474 spheroids formed in 50, 100, and 200 μm microwells ($N = 392, 174, \text{ and } 119$ spheroids, respectively). (f) Quantification of the percentage of microwell area occupied by BT474 spheroids in microwells with different side lengths (50, 100, and 200 μm). Each dot is one spheroid **** $p < 0.0001$ (one-way ANOVA analysis).

CAR T cell cytotoxicity in BT474 spheroids embedded in the 3D matrix compared to the no BG-Herceptin condition (Fig. S4). Finally, we tested the cytotoxic efficacy of our universal CAR system using the T47D breast cancer cell line that has been previously shown to express folate receptor α (FR α).⁵³ In agreement with our results using BG-Herceptin, we found that CAR T cell-mediated cytotoxicity in T47D cancer spheroids was significantly higher following treatment with a BG-conjugated folate receptor α antibody (BG-mirvetuximab⁵⁴) compared to the control without BG-mirvetuximab treatment (Fig. S5).

Next, we used live cell confocal imaging to monitor the dynamic interactions of CAR T cells with BT474 cancer spheroids under both baseline (–BG-Herceptin) and antigen-sensing (+BG-Herceptin) conditions [Figs. 3(a) and 3(b)]. We found that following HER2-sensing,

the fraction of CAR T cells that interacted with cancer spheroids increased over time, with $\sim 73\%$ of the total CAR T cells interacting with cancer spheroids after 12 h [Fig. 3(c)]. Under baseline conditions in the absence of BG-Herceptin, only $\sim 37\%$ of the total CAR T cells interacted with cancer spheroids after 12 h [Fig. 3(c)]. Time-lapse imaging at a focal plane that captured the spheroid core, showed progressive infiltration of CAR T cells when treated with BG-Herceptin, while CAR T cells remained at the periphery of spheroids in the absence of BG-Herceptin treatment [Figs. 3(a) and 3(b)]. To characterize the spatial patterns of CAR T cell trafficking within breast cancer spheroids, we divided each spheroid into three zones as a function of radius: (a) the spheroid periphery (outer zone) (b) the intermediate zone, and (c) the spheroid core (inner zone) [Fig. 3(d)]. We found that

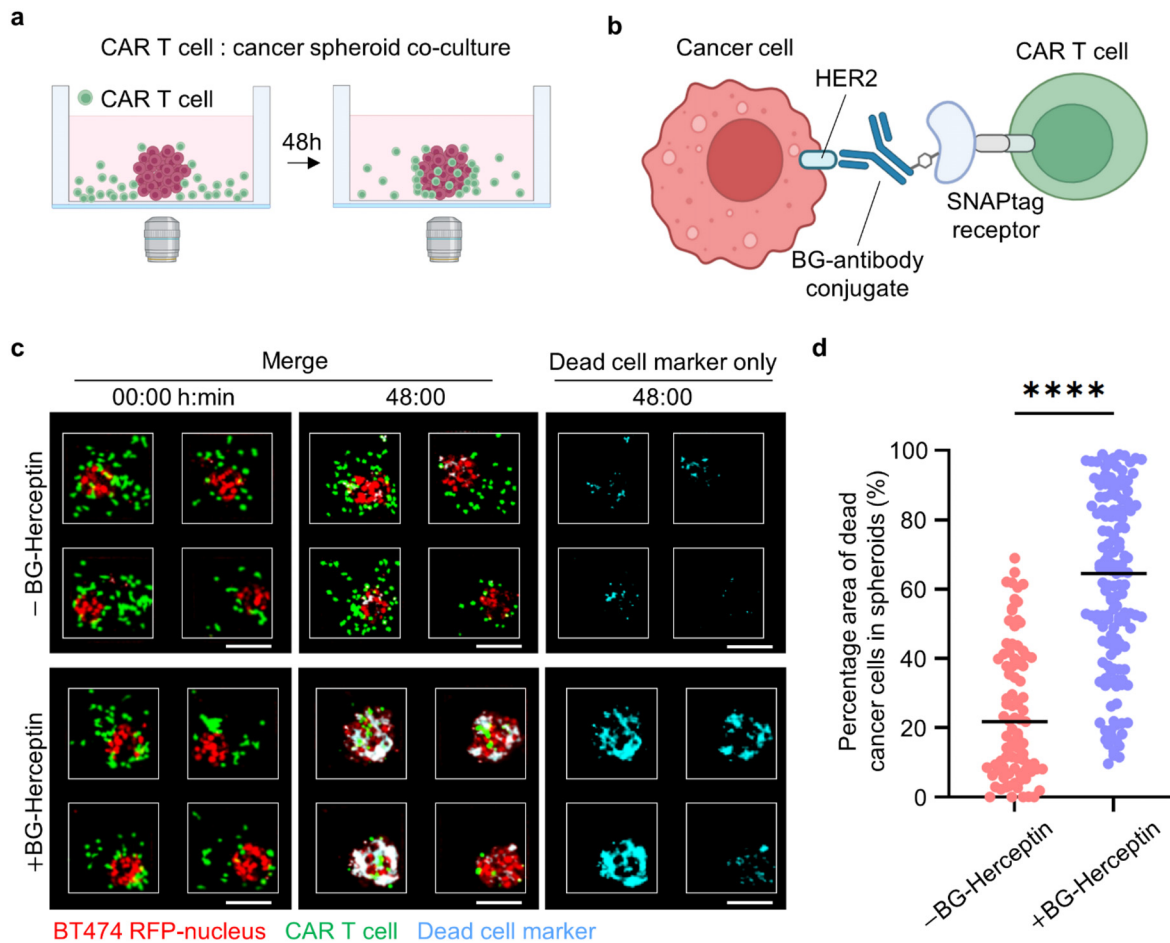


FIG. 2. CAR T cell-mediated cytotoxicity in HER2+ breast cancer spheroids. (a) Setup of CAR T cell and cancer spheroid coculture. (b) Schematics of SNAP-CAR T cells interacting with BG-conjugated antibody adaptor to recognize HER2 antigen on cancer cells. (c) Images showing CAR T cell interactions with BT474 cancer spheroids \pm BG-Herceptin adaptor at 0 and 48 h. Red: BT474-H2BRFP, green: CMFDA dye-stained CAR T cell, and cyan: Sytox deep red cell death dye. Scale bars, 100 μ m. (d) Quantification of cytotoxicity levels, calculated as the overlap area between dead cell markers (Cyan) and cancer cells (RFP) divided by the total RFP area in BT474 cancer spheroids at 48 h. (N = 89 spheroids for -BG-Herceptin and N = 145 spheroids for +BG-Herceptin. Results are representative of three biological replicates.) ****p < 0.0001 (unpaired t-test).

under baseline conditions (-BG-Herceptin), most of the CAR T cells (~90%) remained at the spheroid periphery and there was no significant change in the CAR T cell population within the intermediate zone or spheroid core over time [Fig. 3(e)]. However, following treatment with BG-Herceptin, the distribution of CAR T cells within the spheroid changed over time [Fig. 3(f)]. Notably, 24 h following antigen sensing, a similar population of CAR T cells were present in the periphery (44%) and intermediate (39%) zones, with the lowest population being in the spheroid core (17%) [Fig. 3(f)].

Given previous reports on CAR T cell clustering in two-dimensional assays,²² we assessed the clustering patterns of CAR T cells that had infiltrated within the spheroids and the impact of antigen sensing. Infiltrated CAR T cells within cancer spheroids were classified as single cells [blue in Fig. 4(a)] or clusters [white in Fig. 4(a)]. We found that following 24 h of HER2-sensing (+BG-Herceptin), 13% of infiltrated CAR T cells formed clusters, while only 0.5% of CAR T cells formed clusters under baseline conditions

(-BG-Herceptin) [Fig. 4(b)]. Analysis of the CAR T cell cluster area within cancer spheroids over time showed a rapid increase following treatment with BG-Herceptin [Fig. 4(c)]. Taken together, these results show that sensing of the HER2 antigen promotes CAR T cell-mediated killing of breast cancer cells and stimulates CAR T cell infiltration and cluster formation within cancer spheroids.

Dynamic profiling at the individual spheroid level uncovers predictors of CAR T cell-mediated cytotoxicity with larger spheroid sizes limiting anti-tumor CAR T cell function

Next, we characterized the cytotoxic activity kinetics of CAR T cells that infiltrated within cancer spheroids. Consistent with our endpoint results, we found that BT474 cancer spheroids treated with the BG-Herceptin adaptor exhibited higher levels of cancer cell death for all timepoints compared to the no adaptor condition, with killing

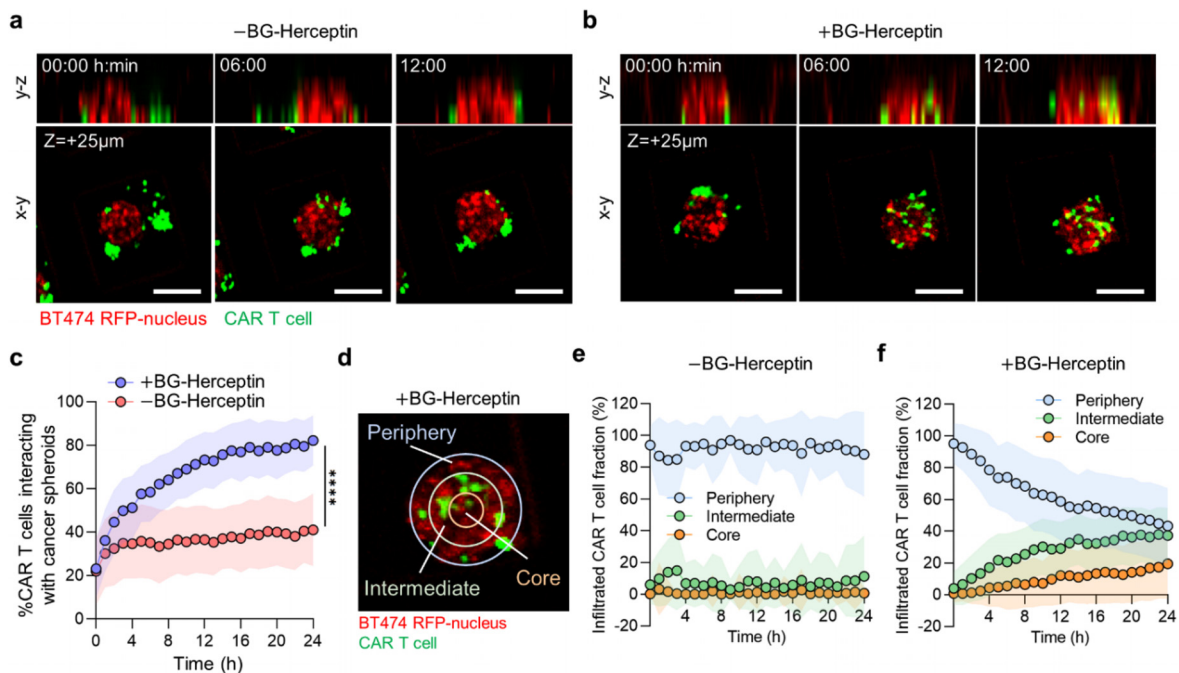


FIG. 3. Sensing of HER2 on breast cancer cells by CAR T cells promotes CAR T cell infiltration within cancer spheroids. (a) and (b) Time-lapse confocal fluorescence imaging of y - z (side view) and x - y (top view) planes of CAR T cell-BT474 spheroid cocultures (a) in the absence and (b) presence of BG-Herceptin (HER2 sensing). Red: BT474 H2B-RFP and green: CMFDA dye-stained CAR T cells. The x - y plane images are captured at $z = +25 \mu\text{m}$ from microwell bottom surface. Scale bars, $100 \mu\text{m}$. (c) Sensing of HER2 increases the percentage of CAR T cells interacting with cancer spheroids. The percentage of interacting CAR T cells was calculated as the GFP area (CAR T cells) overlapping with RFP area (cancer cells) normalized by the total GFP area within a microwell. Plots represent mean \pm SD. $N = 145$ microwells (+BG-Herceptin) and $N = 91$ microwells (-BG-Herceptin). **** $p < 0.0001$ (unpaired t-test analysis). (d) Spatial analysis of CAR T cell infiltration in cancer spheroids divided in three zones as a function of radial position. To define the periphery and intermediate zones, we set the difference between the inner and outer radii at $20 \mu\text{m}$ for each zone, while the core occupied the remaining area of each spheroid. (e) and (f) Spatial distribution of infiltrated CAR T cells over time (e) in the absence of BG-Herceptin and (f) in the presence of BG-Herceptin. Plots represent mean \pm SD. $N = 145$ microwells (+BG-Herceptin) and $N = 91$ microwells (-BG-Herceptin). Results are representative of three biological replicates.

initiated 10 h following HER2 sensing [Figs. 5(a) and 5(b)]. Specifically, under treatment with BG-Herceptin, CAR T cells showed an increased rate of antitumor cytotoxicity over time (1.36% of the tumor cell area killed per hour between 10 and 48 h), compared to the baseline cytotoxicity in the absence of antigen sensing (0.53% of the tumor cell area killed per hour between 10 and 48 h. $p < 0.0001$) [Figs. 5(b) and S6]. Furthermore, this antigen-specific CAR T cell-mediated death was significantly higher than the cancer spheroid-only control that was treated with BG-Herceptin (21.7 fold, $p < 0.0001$) [Fig. 5(b)].

We also evaluated CAR T cell cytotoxic killing at the individual spheroid level. There was significant heterogeneity in the cytotoxic efficacy with a range from 10% to 99% of the tumor cell area that was positive for dead cell markers at 48 h [Fig. 5(c)]. Furthermore, the temporal evolution patterns across spheroids were heterogeneous [Fig. 5(c)]. To identify factors that drive these heterogeneous cytotoxic outcomes, we first compared the microwells with the highest (top quartile with $93\% \pm 4\%$ of the tumor cell area overlapping with dead cell markers) and lowest cytotoxicity [bottom quartile with $26\% \pm 10\%$ of the tumor cell area overlapping with dead cell markers Fig. 5(d)]. We found that the top quartile of microwells with high cytotoxicity exhibited a higher number of initial CAR T cells compared to the bottom quartile [Fig. 5(e)]. Furthermore, the initial spheroid diameter was significantly larger in the bottom quartile microwells, indicating that

cancer cells in larger spheroids are less effectively killed [Fig. 5(f)]. To account for both parameters, we calculated the initial ratio between CAR T cell and spheroid area, which also effectively discriminated between the top quartile of microwells with high cytotoxicity compared to the bottom quartile of microwells with low cytotoxicity [CAR T cell:spheroid area ratio was 1.33 ± 0.5 for the top vs 0.57 ± 0.48 for the bottom quartiles, $p < 0.0001$, Fig. 5(g)]. This relationship was also supported by evaluating the initial CAR T cell:spheroid area ratio and cytotoxicity outcomes across all spheroids (Pearson correlation coefficient $r = 0.57$, $p < 0.001$) [Fig. 5(h)]. We also found a positive correlation between a high initial CAR T cell:spheroid area ratio and high cytotoxicity in the EFM192A breast cancer spheroids (Fig. S7).

To systematically evaluate the effect of spheroid size on CAR T cell cytotoxicity, we seeded BT474 cancer cells at an increasing cell density (0.05×10^6 , 0.2×10^6 , and 0.8×10^6 cells/ml) in microwells. For these seeding densities, we found that mean spheroid diameters ranged from 50 to $200 \mu\text{m}$ [Fig. 5(i)]. A fixed number of CAR T cells (0.2×10^6 cells/ml) was seeded for each cancer cell density resulting in effector to target (E:T) ratios in the range of 4:1, 1:1, and 1:4. Compared to the larger BT474 spheroids (0.8×10^6 cells/ml), we found that smaller spheroids (0.05×10^6 cells/ml) exhibited a twofold higher mean cytotoxicity with values increasing from $43\% \pm 17\%$ to $86\% \pm 15\%$ [Figs. 5(j) and 5(k)]. Next, we used ELISA to quantify the

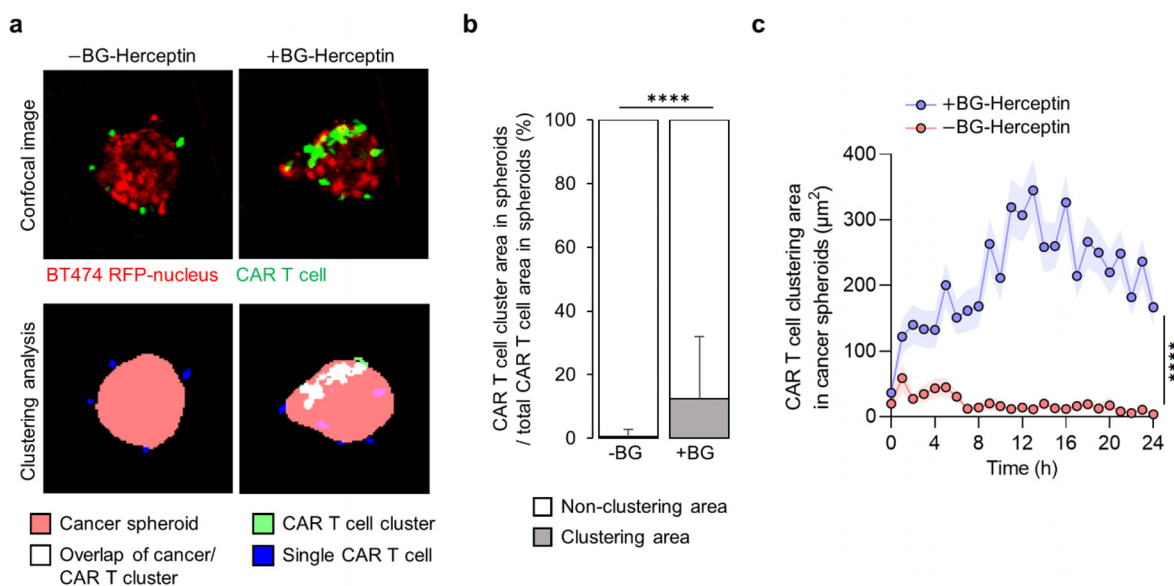


FIG. 4. CAR T cell clustering within breast cancer spheroids depends on HER2 sensing. (a) Image analysis of CAR T cell clustering in cancer spheroids at $z = +25 \mu\text{m}$ focal plane in the absence and presence of BG-Herceptin (HER2 sensing). Images in the top row are fluorescence images and images in the bottom row are segmentations based on cancer spheroid area (red), single CAR T cell area (blue), CAR T cell cluster area (green), and CAR T cell cluster area overlapped with cancer spheroid area (white). (b) Percentage of CAR T cell clustering area over total CAR T cell area in cancer spheroids at $24 \text{ h} \pm \text{BG-Herceptin}$. Mean \pm SD. $N = 145$ microwells (+BG-Herceptin) and $N = 91$ microwells (–BG-Herceptin). (c) The size of CAR T cell cluster area within cancer spheroids increases over time only when HER2 is sensed. Mean \pm sem. $N = 145$ microwells (+BG-Herceptin) and $N = 91$ microwells (–BG-Herceptin). Results are representative of three biological replicates. **** $p < 0.0001$ (unpaired t-test analysis).

concentration of effector cytokines $\text{IFN-}\gamma$ and $\text{TNF-}\alpha$ in culture medium from these microwells with the range of spheroid sizes. We found that $\text{IFN-}\gamma$ and $\text{TNF-}\alpha$ secretion levels were significantly lower for the larger BT474 spheroids (0.8×10^6 cells/ml) compared to the smaller BT474 spheroids (0.05 or 0.2×10^6 cells/ml) [Figs. S8(a) and S8(b)]. As expected, $\text{IFN-}\gamma$ and $\text{TNF-}\alpha$ were only detectable in the presence of BG-Herceptin (indicative of HER2 antigen sensing) [Figs. S8(c) and S8(d)].

To further evaluate the effects of spheroid size on CAR T cell anti-tumor function, we characterized the expression of the granzyme B effector protease in CAR T cells interacting with spheroids of different diameters [Figs. S8(e) and S8(f)]. Consistent with cytotoxicity and the $\text{TNF-}\alpha/\text{IFN-}\gamma$ cytokine findings, we found a higher expression of granzyme B in CAR T cells interacting with smaller spheroids compared to CAR T cells interacting with larger spheroids [Figs. S8(e) and S8(f)]. In addition, we assessed CAR T cell activation using immunofluorescence analysis for CD62L. CD62L is downregulated following T cell activation.⁵⁵ A stronger activation state was indicated by the lower intensity of CD62L in smaller BT474 spheroids compared to larger spheroids [Figs. S8(g) and S8(h)]. Finally, by employing an imaging-based hypoxia sensor, we showed that hypoxia levels increased with cancer spheroid diameter (Fig. S9).

Spatiotemporal analysis of CAR T cell function within the cancer spheroid periphery and core for a fixed cancer spheroid size

Next, we examined the effects of different E:T ratios on anti-tumor CAR T cell function for a fixed cancer spheroid size. We seeded an increasing number of CAR T cells (0.05×10^6 , 0.2×10^6 , 0.8×10^6

cells/ml) in microwells with BT474 spheroids formed at a seeding density of 0.2×10^6 cells/ml and a spheroid diameter $\sim 120 \mu\text{m}$. Under these conditions, E:T ratios ranged from 1:4 to 4:1 for a fixed cancer cell number. Microwells seeded with a higher number of CAR T cells (4:1 E:T) exhibited a threefold higher mean cytotoxic efficiency (73% vs 25%) compared to those seeded with a smaller number of CAR T cells (1:4 E:T) [Fig. 6(a)]. As expected, we found that $\text{IFN-}\gamma$ and $\text{TNF-}\alpha$ secretion levels increased with a higher density of CAR T cells [Figs. 6(b) and 6(c)].

In addition to these global analyses, we investigated the spatial patterns of cytotoxic CAR T cell activity within individual BT474 spheroids (BT474 at 0.2×10^6 cells/ml). In microwells seeded with high CAR T cell density (0.8×10^6 cells/ml), we found a higher number of CAR T cells within the spheroid periphery for both treatment with BG-Herceptin and the baseline conditions [Figs. 6(d) and 6(e)]. However, CAR T cell recruitment within the spheroid core increased only when BG-Herceptin was added to facilitate sensing of the HER2 antigen [Fig. 6(f)]. Tracking of individual CAR T cells within cancer spheroids using live confocal microscopy revealed increased CAR T cell migration speed within the spheroid core compared to the periphery (Fig. S10).

Analysis of CAR T cell-mediated cytotoxicity in the spheroid core compared to the periphery revealed that in the spheroid periphery cancer killing was observed to begin at 10 h, while killing in the spheroid core was delayed to 20 h [Figs. 6(g) and 6(h)]. At the higher CAR T cell seeding density (0.8×10^6 cells/ml), under BG-Herceptin treatment, the killing rates at the periphery and core were comparable [Figs. 6(g) and 6(h)]. However, at a lower CAR T cell seeding density (0.2×10^6 cells/ml), the killing rate at the periphery was higher than the killing rate at the core. Furthermore, consistent with our analysis of cytotoxicity

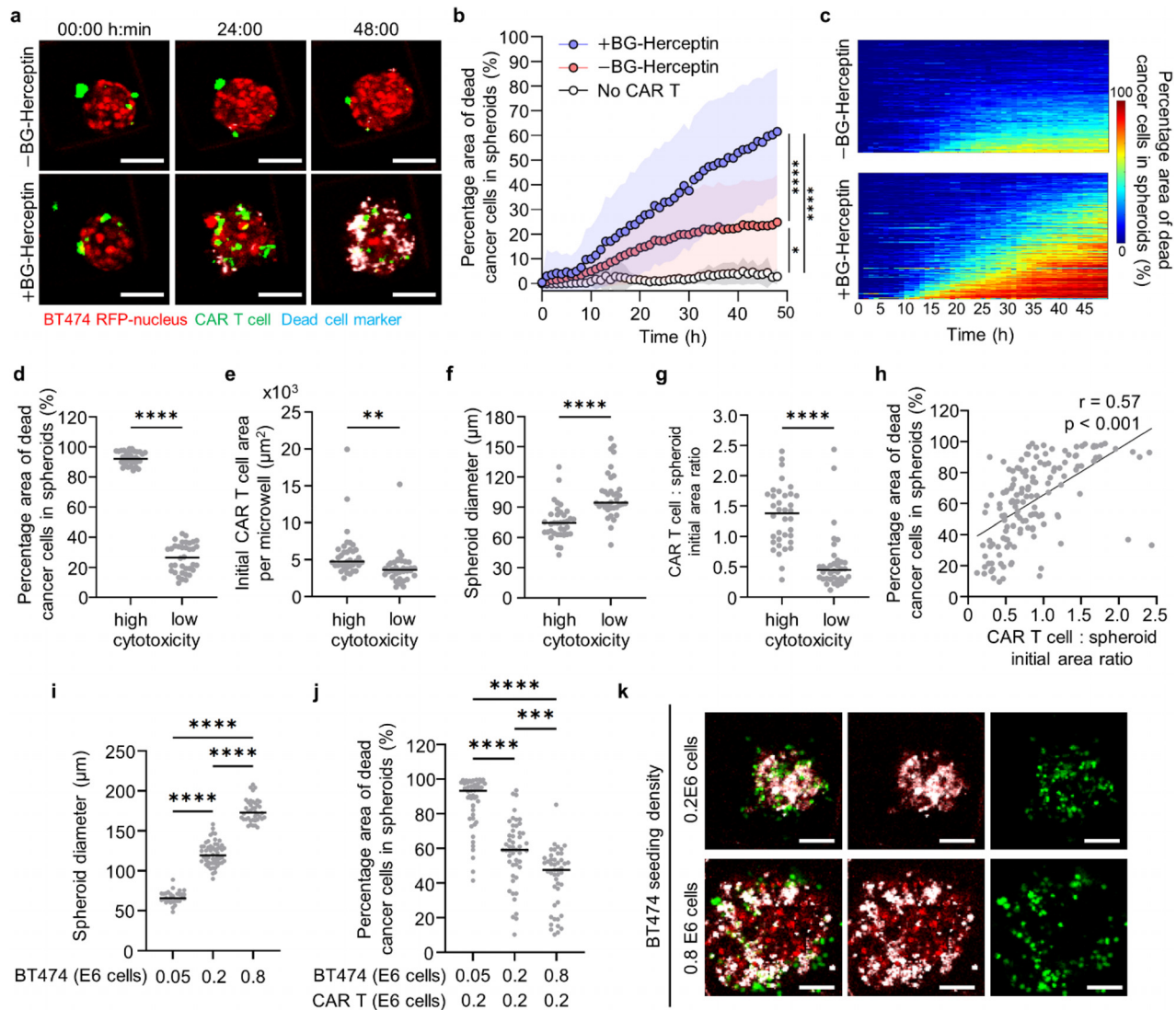


FIG. 5. Dynamic profiling of CAR T cell cytotoxic killing reveals initial CAR T: spheroid ratio as a predictor of antitumor cytotoxicity. (a) Time-lapse confocal fluorescence images of CAR T cell–BT474 spheroid coculture at $z = +25 \mu\text{m}$ in the absence and presence of BG-Herceptin. Red: BT474-H2BRFP, green: CMFDA dye-stained CAR T cells, and cyan: dead cell marker. Scale bars, $100 \mu\text{m}$. (b) Quantification of cytotoxicity levels in BT474 cancer spheroids over time \pm BG-Herceptin. Mean \pm SD (–BG: $N = 91$; +BG: $N = 145$; and no CAR T +BG: $N = 9$ wells). (c) Heatmaps showing the temporal evolution of cytotoxicity for individual spheroids \pm BG-Herceptin [Data from 91 microwells (–BG) and 145 microwells (+BG)]. Each row in the x-axis represents time and columns in the y-axis represent individual microwells. (d)–(g) Each dot is a spheroid and two groups are shown based on high (top quartile) and low (bottom quartile) cytotoxicity levels from +BG-Herceptin condition in panel c. Characterization of (d) cytotoxicity, (e) initial CAR T cell area, (f) initial spheroid diameter, and (g) initial CAR T cell:spheroid area ratio. $**p < 0.01$, $****p < 0.0001$ (unpaired t-tests). (h) Correlation between cytotoxicity and initial CAR T cell:spheroid area ratio in microwells treated with BG-Herceptin ($N = 145$, Pearson correlation coefficient $r = 0.61$, $p < 0.001$). (i) Quantification of spheroid diameter in $300 \times 300 \mu\text{m}$ microwells seeded with different cancer cell numbers. ($N > 30$ spheroids) (one-way ANOVA). $****p < 0.0001$. (j) Quantification of cytotoxicity levels in microwells with different cancer cell seeding densities interacting with a fixed number of CAR T cells in the presence of BG-Herceptin ($N > 46$ spheroids from three biological replicates) (One-way ANOVA) $****p < 0.0001$, $****p < 0.0001$. (k) Representative images of cancer spheroids with different seeding densities interacting with CAR T cells in the presence of BG-Herceptin at 48 h. Red: BT474-H2BRFP, green: CMFDA dye-stained CAR T cells, and cyan: dead cell marker. Scale bars, $50 \mu\text{m}$.

predictors [Fig. 5(h)], we found that increasing the CAR T cell seeding density within the microwell resulted in a higher initial CAR T cell:spheroid area ratio (2.9 ± 2.7) that was also associated with higher cytotoxicity (Fig. S11). These results show that antigen-specific CAR T cell–tumor cell interactions promote CAR T cell infiltration within the 3D spheroid core and subsequent tumor cell killing.

DISCUSSION

The solid tumor microenvironment poses a significant barrier that CAR T cells must overcome to detect and kill cancer cells. Experimental models that recapitulate different features of solid tumors are needed to understand CAR T cell trafficking and test their antitumor efficacy. Here, we developed a microwell-based platform to

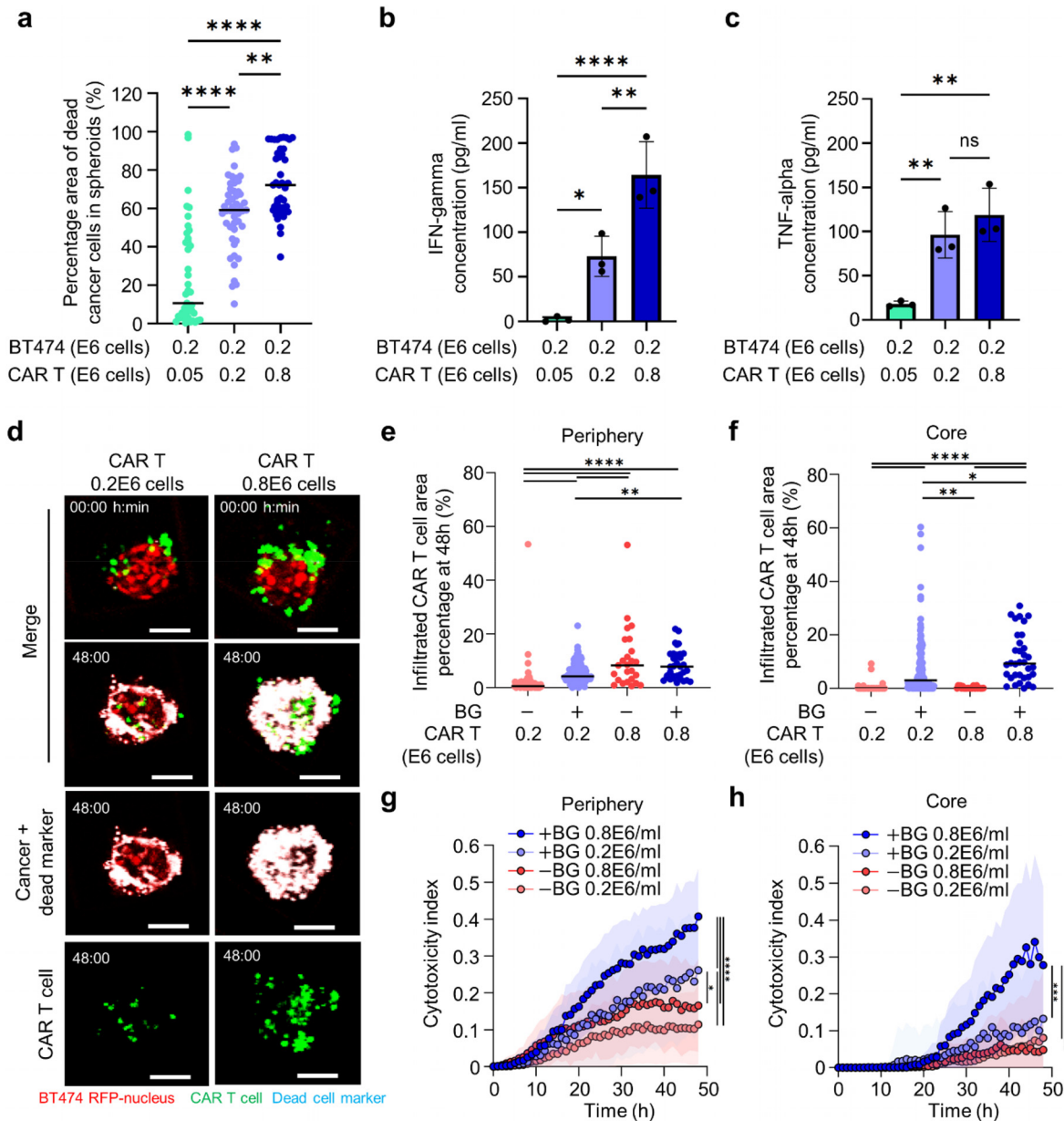


FIG. 6. CAR T cell cytotoxicity within the spheroid core is enhanced by higher CAR T cell density when HER2 antigen is recognized. (a) Quantification of cytotoxicity in microwells seeded with different CAR T cell numbers for a fixed cancer seeding density in the presence of BG-Herceptin ($N > 41$ spheroids from three biological replicates) (one-way ANOVA) $**p < 0.01$, $****p < 0.0001$. (b) and (c) Characterization of (b) IFN- γ and (c) TNF- α secretion in microwells with different CAR T cell seeding densities. Three biological replicates (one-way ANOVA) $*p < 0.05$, $**p < 0.01$, and $****p < 0.0001$. (d) Time-lapse confocal fluorescence imaging of CAR T cell-BT474 spheroid coculture in the presence of BG-Herceptin with different seeding densities (low: 0.2×10^6 cells/ml and high: 0.8×10^6 cells/ml) at 0 and 48 h. Red: BT474-H2BRFP, green: CMFDA dye-stained CAR T cells, and cyan: dead cell markers. Scale bars, $100 \mu\text{m}$. (e) and (f) Quantification of the percentage of infiltrated CAR T cells out of the total CAR T cells in each spheroid at (e) the periphery and (f) in the core at $48 \text{ h} \pm$ BG-Herceptin with different CAR T cell seeding densities. (g) and (h) Cytotoxic index (definition in Methods) in (g) spheroid periphery and (h) core \pm BG-Herceptin. Plots represent mean \pm SD. -BG low ($N = 91$), +BG low ($N = 145$), -BG high ($N = 25$), and +BG high ($N = 34$). $*p < 0.05$, $**p < 0.01$, and $***p < 0.001$ $****p < 0.0001$ (one-way ANOVA analysis).

quantitatively assess CAR T cell infiltration and cytotoxic functions in 3D HER2+ breast cancer spheroids. By profiling individual cancer spheroids, we identified the initial CAR T cell:spheroid area ratio as a predictor of CAR T cell-mediated killing. Furthermore, using

spatiotemporal analysis of CAR T cell trafficking, we showed that HER2 antigen sensing promotes CAR T cell clustering and infiltration within the 3D spheroid core. These results demonstrate the capabilities of our microwell assay as a miniaturized technology to elucidate

dynamic cell–cell interactions at play during CAR T cell anti-tumor functions.

Spheroids enable the study of physiologically relevant parameters, including spatial zonation and cell motility within a multicellular environment, which is not feasible in 2D models.⁵⁶ Studies using cancer spheroids have yielded insight into drug distribution as a function of distance from the spheroid core^{35,57} and heterotypic tumor–immune cell interactions.^{58,59} Compared to the traditional suspension culture methods (e.g., hanging drop and ultra-low adhesion surfaces), integrating spheroids within microfabricated platforms provides advantages with respect to controlling cell seeding and the extracellular environment.⁶⁰ For example, microfluidic devices with cancer spheroids embedded in a 3D matrix facilitated the analysis of directional T cell trafficking and cytotoxic activity.^{37,38,61} Evaluation of targeted therapies (e.g., G9a/GLP inhibitors) to stimulate T cell cytotoxicity in 3D microfluidic models has been shown to reflect *in vivo* therapeutic outcomes.⁶² With respect to monitoring real-time tumor–immune cell crosstalk, our microwell platform offers several critical features. First, spheroids are spatially segregated to facilitate parallel comparisons between a large number of wells in a single experiment. Second, 3D spheroids are formed in a microwell with controlled size. Finally, by controlling the cell seeding sequence, we avoid transferring cancer spheroids between culture platforms prior to high-resolution imaging.

Cell migration in a complex 3D microenvironment^{63,64} is critical for the engagement of cytotoxic T cells that target tumor cells.^{37,62,65} We utilized universal adaptor CAR T cells to study antigen-specific effects on migration under the control of an adaptor molecule. We found that CAR T cell infiltration and clustering within cancer spheroids was enhanced following the sensing of HER2 on cancer cells. These antigen-specific effects may promote cooperation among CAR T cells via paracrine signaling as shown by a previous study using cytotoxic T cells. This study employed 3D macroscale cultures to also demonstrate that engagement of cognate targets by cytotoxic T cells promotes swarming.⁶¹ These cooperative interactions between T cells following antigen recognition were also shown using a microfluidic droplet assay with melanoma spheroids and ovalbumin-targeted murine OT-I cytotoxic T cells.⁶¹ Furthermore, we found that CAR T cells localized within the spheroid core only in the presence of the HER2 antibody adaptor and irrespective of the CAR T cell seeding density, consistent with a previous study that observed CAR T cell infiltration in HER2 therapy-resistant tumor spheroids.⁶⁶ In addition, our results agree with a previous *in vitro* study that reported clustering under 2D conditions when comparing mock-transduced CAR T cells with anti-BCMA (B-cell maturation antigen) targeted CAR T cells.²² These results provide further supportive evidence for the critical role of antigen-specific tumor–immune crosstalk that mediates CAR T cell trafficking in a 3D environment.

Sustained CAR T cell cytotoxic activity represents a major challenge in developing CAR T cell therapies against solid tumors.^{67,68} By monitoring CAR T cell-mediated tumor cell killing at the individual spheroid level, we showed the suppressive effects of spheroid size and that the initial CAR T cell to spheroid area ratio can serve as a predictor of cytotoxicity. These results agree with a previous study that showed killing of B16 melanoma cells expressing SIINFEKL as a function of initial OT-I T cell concentration.⁶⁹ Furthermore, our findings revealed that for a fixed number of CAR T cells, increasing spheroid size reduced cytokine secretion, despite the higher surface area for

tumor–CAR T cell interactions. Under these conditions, the E:T ratio was lower for the larger spheroid sizes and our findings are consistent with a previous study showing lower killing efficiency and cytokine secretion when the E:T ratio was decreased.⁷⁰ Another study employed intravital imaging and demonstrated that a high local density of OT-I cytotoxic T cells correlated with a lower number of virus-infected cells *in vivo*.⁷¹ Furthermore, we characterized the hypoxic state across the range of spheroids formed in our microwells, and consistent with a previous study in hepatocytes, we found that larger spheroids exhibited lower oxygen levels.²⁷ It is also important to monitor cytotoxic T cell function in spatial zones that have been associated with poor T cell infiltration, such as the intratumor core.^{72,73} Using spatiotemporal analysis of killing dynamics in our microwell platform, we showed that HER2+ cancer cells within the spheroid core could be eliminated by CAR T cells in an antigen-specific manner. Our results are consistent with a previous study that formed HER2 therapy-resistant JIMT1 spheroids using ultra-low adhesion 96-well plates and evaluated cytotoxicity using anti-HER2 CAR T cells.³²

In the multicellular microenvironment of solid tumors, CAR T cells migrate within a 3D extracellular matrix prior to killing cancer cells.^{37,62} Spheroids in our microwell platform are not surrounded by an extracellular matrix and thus CAR T cells only migrate within the 3D tumor spheroid. However, we found that HER2 antigen-mediated CAR T cell cytotoxicity was qualitatively similar between microwell-based spheroids and spheroids embedded in a 3D collagen matrix (Fig. S4). Furthermore, our experimental design included only cancer cells and CAR T cells; thus, future studies should evaluate the role of abundant stromal cell types in solid tumors (e.g., fibroblasts) on antigen-specific CAR T cell function. Finally, our experiments were performed on a short timescale (48 h). Future investigations should evaluate the impact of antigen recognition on T cell activation state (e.g., using a panel of markers including CD69 and CD25) and CAR T cell programmed death at longer timescales.⁷⁴

In summary, we present a microwell platform to quantitatively study CAR T cell infiltration and cytotoxicity in HER2 breast cancer spheroids as a function of spheroid size. Our findings reveal distinct patterns of anti-tumor T cell functions within the spheroid periphery compared to the spheroid core that are dependent on the engagement of the HER2 antigen on tumor cells. The universal CAR T cell system used in our study provides flexibility in directing CAR T cells against antigens that can be targeted using a benzylguanine-conjugated antibody. Finally, our multiwell plate-compatible assay can be integrated into combinatorial drug screening platforms and the miniaturized scale offers advantages for studying low-volume, patient-derived samples.

METHODS

PDMS microwell fabrication and assembly

SU-8 silicon wafers served as molds for PDMS microwell fabrication with a side length of 50, 100, and 200 μm . The height of the microwell was 100 μm . An LCD-based Phrozen Sonic Mini 4K resin printer was used for the fabrication of microwells with a side length of 300 μm and a height of 300 μm using a previously published method.⁷⁵ PDMS was mixed in a 10:1 ratio of elastomer base to curing agent and placed in a vacuum desiccator for one hour to degas. Then, 2.5 g of the PDMS mixture was poured on the center of the microwell mold. The mold was fixed on a spin-coater and rotated at 1000 rpm for 5 min.

Next, the mold was incubated overnight in an 80 °C oven. Subsequently, the thin PDMS microwell sheet was peeled off and plasma-bonded into each well of a 24-well glass-bottom plate. After incubating the plate in an 80 °C oven for 10 min, the plate was treated with plasma once more, and 500 μ l of 2% pluronic solution was added to each well. The plate was then centrifuged at 900 rpm for 5 min to remove any bubbles trapped in the microwells. After incubating the plate in the incubator for one hour, it was washed three times with PBS and once with cell culture medium before seeding the cells.

3D spheroid formation and CAR T cell transduction

The human breast cancer cell lines BT474, EFM192A (expressing fluorescent nuclear marker H2B-RFP⁷⁶), and T47D were cultured in RPMI supplemented with 10% heat inactivated fetal bovine serum (HIFBS) and 1% penicillin/streptomycin. A cancer cell seeding solution at a density of 0.2×10^6 cells/ml was prepared and subsequently 1 ml of the cancer cell solution was added to each well of a 24-well glass-bottom plate. The plate was centrifuged at 900 rpm for 1 min to promote cancer cell settling within the microwells. We allowed 72 h for spheroids to form in a 5% CO₂ and 37 °C incubator.

CAR T cells were generated by following a protocol described in our previous studies.⁴⁰ In brief, CD3+ T cells isolated with Pan T cell isolation kit (Miltenyi Biotec), were stimulated with TransAct Human T cell activation reagent (Miltenyi Biotec), 100 U/ml human IL-2 IS (Miltenyi Biotec), and 1 ng/ml IL-15 (Miltenyi Biotec) for 48 h. For lentiviral transduction, the viral vector-containing medium was spun down in a retronectin coated plate at 2000 \times g for 2 h at 32 °C, and after removing 2 ml of supernatant, 1×10^6 of T cells were added in 4 ml of media and spun down for an additional 10 min 1000 \times g at 32 °C. Cells were then expanded every 2–3 days, and fresh IL-2 and IL-15 were added in each expansion time. Transduction efficiency was tested at day 8 post-transduction (Fig. S12).

Production of BG-conjugated antibodies

The anti-HER2 antibody trastuzumab (Herceptin, Genentech) and anti-folate receptor α antibody mirvetuximab were conjugated to BG following the protocol described in our previous studies.⁴⁰ In brief, Herceptin was buffer exchanged in PBS by using 7 K MWCO Zeba Spin Desalting Columns (ThermoFisher Scientific). Then it was incubated with 20ME (molar equivalent) of BG-GLA-NHS (NEB) for 30 min at room temperature, subsequently buffer exchanged by using 7 K MWCO Zeba Spin Desalting Columns, and the concentration was measured by Nanodrop One (ThermoFisher Scientific).

CAR T cell-spheroid interaction assays

Before seeding CAR T cells, we carefully aspirated the media from the microwells containing cancer spheroids and added 500 μ l of RPMI media supplemented with a 1:5000 dilution of SYTOXTM Deep Red Nucleic Acid Stain dye (#S11381, Invitrogen) for tracking dead cells. To quantify CAR T cell numbers, we performed staining with 10 ng/ml CellTracker Green CMFDA Dye (#C7025, Fisher) for 25 min at 37 °C and washed once with RPMI. Subsequently, we added 0.2E6/ml CAR T cells in 500 μ l of RPMI supplemented with BG-Herceptin to each microwell at a final concentration of 1 μ g/ml for +BG-Herceptin samples. For the higher initial CAR T cell seeding density, we added a four time higher concentration at 0.8E6/ml CAR T cells to

the microwells. The cancer spheroid-only condition (no CAR T cells added) also included a concentration of 1 μ g/ml of BG-Herceptin.

Time-lapse confocal microscopy

For time-lapse imaging, the microwell plate was mounted on a Zeiss LSM700 confocal microscope housed within the Tokai-Heat incubation system. Live images were captured as a z-stack (3 stacks with a 25 μ m interval starting from the bottom of the microwell surface) every hour for 48 h using a 10 \times 0.45 NA objective lens.

Image analysis

MATLAB was utilized for image analysis. To quantify CAR T cell cytotoxicity, we calculated the overlap area of RFP+ (cancer cells expressing H2B-RFP) and Cy5+ (dead cell marker, shown as cyan in figures for visibility) and divided it by the total RFP+ area. We then multiplied it by 100 to convert into a percentage.

To enable whole cancer spheroid segmentation for spatial analysis, we applied a 20 pixel median filter on the RFP images to group cancer cell nuclei into a single object prior to intensity thresholding. GFP (CAR T cells) and Cy5 images were also segmented through intensity thresholding. The percentage of CAR T cells interacting with cancer spheroids was determined by calculating the overlap area between the cancer spheroid area (RFP) and the CAR T cell area (GFP), divided by the total CAR T cell area (GFP) per microwell. The total CAR T cell area was computed by summing the GFP area within the microwell over the entire z-stacks. To characterize CAR T cell clustering areas, we first identified GFP objects with an area above 50 pixels (312.5 μ m²), comprising approximately ≥ 4 cells, as a CAR T cell cluster. The remaining GFP objects were classified as single CAR T cells. We also report the percentage of CAR T cells that were organized in a cluster by calculating the ratio of the overlap between the cancer spheroid area and the CAR T cluster area, divided by the overlap between the cancer spheroid area and the total CAR T cell area. We report a cytotoxicity index to compare cytotoxicity in the core vs the periphery region of each cancer spheroid. The cytotoxicity index was calculated as the overlap area between the cancer spheroid area and dead cell area, divided by the total cancer spheroid area.

Enzyme-linked immunosorbent assay (ELISA)

Conditioned medium was collected 48 hours post seeding CAR T cells in a microwell plate. IFN- γ and TNF- α levels in the conditioned medium were quantified with corresponding ELISA kits (IFN- γ (cat# DY285B-05, R&D Systems) and TNF- α (cat# DY210-05, R&D Systems)). Kits were performed according to the manufacturer's instructions. The absorbance was measured using Synergy LX (Agilent) at 450 nm and the absorbance at 540 nm was subtracted to correct for any plate abnormalities. The sample concentration was calculated using a standard curve of recombinant human TNF- α or IFN- γ using Prism (Version 9.0, GraphPad Software).

Immunofluorescence staining analysis

Spheroids were harvested from the microwells and transferred to 15 ml centrifuge tubes. After centrifugation (70 g, 5 min), the media was carefully aspirated, and spheroids were fixed in 4% paraformaldehyde (PFA) overnight at 4 °C. Following another centrifugation

(70 g, 2 min), the PFA was carefully aspirated, and spheroids were incubated in 1 ml of a buffer [LI-COR Intercept (cat # NC1660556, Fisher) containing 0.1% Triton X-100] for 15 min at 4 °C. After centrifugation (70 g, 2 min), the supernatant was carefully aspirated, 200 μ l of buffer was added and transferred to a non-tissue culture treated 24-well plate. Primary antibodies were mixed in 200 μ l of buffer, added to the samples in the 24-well plate, and incubated overnight at 4 °C using a shaker. Next, 1 ml of buffer was added to spheroids and incubated for 1 h at room temperature. The plate was tilted, and 1.2 ml of buffer was carefully removed, and another 1 ml of fresh buffer was added. After 1 h of incubation at room temperature, this washing step was repeated three times. Secondary antibodies were added in 200 μ l of buffer and incubated overnight at 4 °C using a shaker. The same washing step was repeated. Finally, the samples were collected in 15 ml centrifuge tubes and centrifuged (70 g, 5 min). Samples were transferred to a glass-bottom dish for confocal imaging.

Statistical analysis

For statistical analyses involving multiple groups, we applied one-way analysis of variance (ANOVA) and Tukey's *post hoc* test for multiple comparisons. Two group comparisons were conducted using an unpaired t-test using Prism. The statistical significance is marked by asterisks in the figures, and we considered P-values below 0.05 as significant.

SUPPLEMENTARY MATERIAL

See the [supplementary material](#) for additional information on spheroid formation of EFM192A cells (Fig. S1), separate fluorescent channel images of CAR T-BT474 spheroid cocultures (Fig. S2), EFM192A spheroid cytotoxicity measurement (Fig. S3), ECM-embedding experiment (Fig. S4), T47D spheroid cytotoxicity measurement (Fig. S5), cytotoxicity rate measurement (Fig. S6), correlation between cytotoxicity and initial CAR T cell: EFM192A spheroid area (Fig. S7), characterization of CAR T cell function in microwells with different BT474 seeding densities (Fig. S8), hypoxic state characterization (Fig. S9), CAR T cell migration analysis (Fig. S10), CAR T cell seeding density effect on cytotoxicity (Fig. S11), and flow cytometry characterization of CAR T cell transduction (Fig. S12).

ACKNOWLEDGMENTS

This work was supported by the National Cancer Institute (R00CA222554 to I.K.Z.), the National Cancer Center Postdoctoral Fellowship (to Y.C.), the NIH grant R01 GM142007 (to J.L.), a Magee Women's Research Institute Breast Cancer pilot grant, the UPMC Hillman Cancer Center, and the Department of Bioengineering, Swanson School of Engineering at the University of Pittsburgh.

AUTHOR DECLARATIONS

Conflict of Interest

Yes, J.L. is an inventor on a patent application filed by the University of Pittsburgh on the universal SNAP-CAR technology used herein (WO2020072764A1). The remaining authors declare no competing interest.

Ethics Approval

Ethics approval is not required.

Author Contributions

Youngbin Cho: Conceptualization (equal); Data curation (equal); Formal analysis (equal); Funding acquisition (equal); Investigation (equal); Methodology (equal); Software (equal); Visualization (equal); Writing – original draft (equal); Writing – review & editing (equal). **Matthew Laird:** Investigation (equal); Methodology (equal). **Teddi Bishop:** Investigation (equal); Methodology (equal). **Ruxuan Li:** Methodology (equal). **Dorota E. Jazwinska:** Investigation (supporting); Writing – review & editing (supporting). **Elisa Ruffo:** Conceptualization (equal); Investigation (equal); Resources (equal); Writing – review & editing (equal). **Jason Lohmueller:** Conceptualization (equal); Funding acquisition (equal); Investigation (equal); Resources (equal); Writing – review & editing (equal). **Ioannis K. Zervantonakis:** Conceptualization (equal); Funding acquisition (equal); Investigation (equal); Methodology (equal); Resources (equal); Supervision (equal); Writing – original draft (equal); Writing – review & editing (equal).

DATA AVAILABILITY

The data that support the findings of this study are available from the corresponding author upon reasonable request.

REFERENCES

- M. P. Jogalekar, R. L. Rajendran, F. Khan, C. Dmello, P. Gangadaran, and B. C. Ahn, "CAR T-cell-based gene therapy for cancers: New perspectives, challenges, and clinical developments," *Front. Immunol.* **13**, 925985 (2022).
- H. Dai, Y. Wang, X. Lu, and W. Han, "Chimeric antigen receptors modified T-Cells for cancer therapy," *J. Natl. Cancer Inst.* **108**, djv439 (2016).
- D. J. Baker, Z. Arany, J. A. Baur, J. A. Epstein, and C. H. June, "CAR T therapy beyond cancer: The evolution of a living drug," *Nature* **619**, 707–715 (2023).
- R. J. Brentjens, M. L. Davila, I. Riviere, J. Park, X. Wang, L. G. Cowell, S. Bartido, J. Stefanski, C. Taylor, M. Olszewska, O. Borquez-Ojeda, J. Qu, T. Wasielewska, Q. He, Y. Bernal, I. V. Rijo, C. Hedvat, R. Kobos, K. Curran, P. Steinherz, J. Jurcic, T. Rosenblatt, P. Maslak, M. Frattini, and M. Sadelain, "CD19-targeted T cells rapidly induce molecular remissions in adults with chemotherapy-refractory acute lymphoblastic leukemia," *Sci. Transl. Med.* **5**, 177ra138 (2013).
- D. W. Lee, J. N. Kochenderfer, M. Stetler-Stevenson, Y. K. Cui, C. Delbrook, S. A. Feldman, T. J. Fry, R. Orentas, M. Sabatino, N. N. Shah, S. M. Steinberg, D. Stronck, N. Tschernia, C. Yuan, H. Zhang, L. Zhang, S. A. Rosenberg, A. S. Wayne, and C. L. Mackall, "T cells expressing CD19 chimeric antigen receptors for acute lymphoblastic leukaemia in children and young adults: A phase 1 dose-escalation trial," *Lancet* **385**, 517–528 (2015).
- J. H. Park, I. Riviere, M. Gonen, X. Wang, B. Sènèchal, K. J. Curran, C. Sauter, Y. Wang, B. Santomasso, E. Mead, M. Roshal, P. Maslak, M. Davila, R. J. Brentjens, and M. Sadelain, "Long-term follow-up of CD19 CAR therapy in acute lymphoblastic leukemia," *N. Engl. J. Med.* **378**, 449–459 (2018).
- G. L. Beatty and M. O'Hara, "Chimeric antigen receptor-modified T cells for the treatment of solid tumors: Defining the challenges and next steps," *Pharmacol. Ther.* **166**, 30–39 (2016).
- G. Guzman, M. R. Reed, K. Bielamowicz, B. Koss, and A. Rodriguez, "CAR-T therapies in solid tumors: opportunities and challenges," *Curr. Oncol. Rep.* **25**, 479–489 (2023).
- D. T. Nguyen, E. Ogando-Rivas, R. Liu, T. Wang, J. Rubin, L. Jin, H. Tao, W. W. Sawyer, H. R. Mendez-Gomez, M. Cascio, D. A. Mitchell, J. Huang, W. G. Sawyer, E. J. Sayour, and P. Castillo, "CAR T cell locomotion in solid tumor microenvironment," *Cells* **11**, 1974 (2022).

- ¹⁰A. Schmidts and M. V. Maus, "Making CAR T cells a solid option for solid tumors," *Front. Immunol.* **9**, 2593 (2018).
- ¹¹A. K. Grosskopf, L. Labanieh, D. D. Klysz, G. A. Roth, P. Xu, O. Adebawale, E. C. Gale, C. K. Jons, J. H. Klich, J. Yan, C. L. Maikawa, S. Correa, B. S. Ou, A. I. d'Aquino, J. R. Cochran, O. Chaudhuri, C. L. Mackall, and E. A. Appel, "Delivery of CAR-T cells in a transient injectable stimulatory hydrogel niche improves treatment of solid tumors," *Sci. Adv.* **8**, eabn8264 (2022).
- ¹²M. Hong, S. Talluri, and Y. Y. Chen, "Advances in promoting chimeric antigen receptor T cell trafficking and infiltration of solid tumors," *Curr. Opin. Biotechnol.* **84**, 103020 (2023).
- ¹³M. Jonnalagadda, A. Mardiros, R. Urak, X. Wang, L. J. Hoffman, A. Bernanke, W. C. Chang, W. Bretzlaff, R. Starr, S. Priceman, J. R. Ostberg, S. J. Forman, and C. E. Brown, "Chimeric antigen receptors with mutated IgG4 Fc spacer avoid Fc receptor binding and improve T cell persistence and antitumor efficacy," *Mol. Ther.* **23**, 757–768 (2015).
- ¹⁴S. J. Priceman, E. A. Gerds, D. Tilakawardane, K. T. Kennewick, J. P. Murad, A. K. Park, B. Jeang, Y. Yamaguchi, X. Yang, R. Urak, L. Weng, W. C. Chang, S. Wright, S. Pal, R. E. Reiter, A. M. Wu, C. E. Brown, and S. J. Forman, "Co-stimulatory signaling determines tumor antigen sensitivity and persistence of CAR T cells targeting PSCA+ metastatic prostate cancer," *Oncoimmunology* **7**, e1380764 (2018).
- ¹⁵M. Cazaux, C. L. Grandjean, F. Lemaitre, Z. Garcia, R. J. Beck, I. Milo, J. Postat, J. B. Beltman, E. J. Cheadle, and P. Bousso, "Single-cell imaging of CAR T cell activity in vivo reveals extensive functional and anatomical heterogeneity," *J. Exp. Med.* **216**, 1038–1049 (2019).
- ¹⁶I. A. Cockburn, R. Amino, R. K. Kelemen, S. C. Kuo, S. W. Tse, A. Radtke, L. Mac-Daniel, V. V. Ganusov, F. Zavala, and R. Ménard, "In vivo imaging of CD⁸⁺ T cell-mediated elimination of malaria liver stages," *Proc. Natl. Acad. Sci. U. S. A.* **110**, 9090–9095 (2013).
- ¹⁷P. Luangwattananun, M. Junking, J. Sujitjooon, Y. Wutti-In, N. Pongvarin, C. Thuwajit, and P. T. Yenchitsomanus, "Fourth-generation chimeric antigen receptor T cells targeting folate receptor alpha antigen expressed on breast cancer cells for adoptive T cell therapy," *Breast Cancer Res. Treat.* **186**, 25–36 (2021).
- ¹⁸R. Zhou, M. Yazdanifar, L. D. Roy, L. M. Whilding, A. Gavrill, J. Maher, and P. Mukherjee, "CAR T cells targeting the tumor MUC1 glycoprotein reduce triple-negative breast cancer growth," *Front. Immunol.* **10**, 1149 (2019).
- ¹⁹G. Liu, W. Rui, H. Zheng, D. Huang, F. Yu, Y. Zhang, J. Dong, X. Zhao, and X. Lin, "CXCR2-modified CAR-T cells have enhanced trafficking ability that improves treatment of hepatocellular carcinoma," *Eur. J. Immunol.* **50**, 712–724 (2020).
- ²⁰Y. Liu, Y. Zhou, K. H. Huang, Y. Li, X. Fang, L. An, F. Wang, Q. Chen, Y. Zhang, A. Shi, S. Yu, and J. Zhang, "EGFR-specific CAR-T cells trigger cell lysis in EGFR-positive TNBC," *Aging* **11**, 11054–11072 (2019).
- ²¹C. Guo, E. Dong, Q. Lai, S. Zhou, G. Zhang, M. Wu, X. Yue, Y. Tao, Y. Peng, J. Ali, Y. Lu, Y. Fu, W. Lai, Z. Zhang, F. Ma, Y. Yao, L. Gou, H. Yang, and J. Yang, "Effective antitumor activity of 5T4-specific CAR-T cells against ovarian cancer cells in vitro and xenotransplanted tumors in vivo," *MedComm* **1**, 338–350 (2020).
- ²²X. Wang, I. Scarfo, A. Schmidts, M. Toner, M. V. Maus, and D. Irimia, "Dynamic profiling of antitumor activity of CAR T cells using micropatterned tumor arrays," *Adv. Sci.* **6**, 1901829 (2019).
- ²³S. Raghavan, M. R. Ward, K. R. Rowley, R. M. Wold, S. Takayama, R. J. Buckanovich, and G. Mehta, "Formation of stable small cell number three-dimensional ovarian cancer spheroids using hanging drop arrays for preclinical drug sensitivity assays," *Gynecol. Oncol.* **138**, 181–189 (2015).
- ²⁴S. Raghavan, P. Mehta, E. N. Horst, M. R. Ward, K. R. Rowley, and G. Mehta, "Comparative analysis of tumor spheroid generation techniques for differential in vitro drug toxicity," *Oncotarget* **7**, 16948–16961 (2016).
- ²⁵M. S. Lam, J. J. Aw, D. Tan, R. Vijayakumar, H. Y. G. Lim, S. Yada, Q. Y. Pang, N. Barker, C. Tang, B. T. Ang, R. M. Sobota, and A. Pavesi, "Unveiling the influence of tumor microenvironment and spatial heterogeneity on temozolomide resistance in glioblastoma using an advanced human in vitro model of the blood-brain barrier and glioblastoma," *Small* **19**, e2302280 (2023).
- ²⁶R. L. F. Amaral, M. Miranda, P. D. Marcato, and K. Swiech, "Comparative analysis of 3D bladder tumor spheroids obtained by forced floating and hanging drop methods for drug screening," *Front. Physiol.* **8**, 605 (2017).
- ²⁷R. Glicklis, J. C. Merchuk, and S. Cohen, "Modeling mass transfer in hepatocyte spheroids via cell viability, spheroid size, and hepatocellular functions," *Biotechnol. Bioeng.* **86**, 672–680 (2004).
- ²⁸K. M. Tevis, R. J. Cecchi, Y. L. Colson, and M. W. Grinstaff, "Mimicking the tumor microenvironment to regulate macrophage phenotype and assessing chemotherapeutic efficacy in embedded cancer cell/macrophage spheroid models," *Acta Biomater.* **50**, 271–279 (2017).
- ²⁹G. Al-Hity, F. Yang, E. Campillo-Funollet, A. E. Greenstein, H. Hunt, M. Mampay, H. Intabli, M. Falcinelli, A. Madzvamuse, C. Venkataraman, and M. S. Flint, "An integrated framework for quantifying immune-tumour interactions in a 3D co-culture model," *Commun. Biol.* **4**, 781 (2021).
- ³⁰T. Courau, J. Bonnereau, J. Chicoteau, H. Bottois, R. Remark, L. Assante Miranda, A. Toubert, M. Blery, T. Aparicio, M. Allez, and L. Le Bourhis, "Cocultures of human colorectal tumor spheroids with immune cells reveal the therapeutic potential of MICA/B and NKG2A targeting for cancer treatment," *J. Immunother. Cancer* **7**, 74 (2019).
- ³¹Y. Song, C. Tong, Y. Wang, Y. Gao, H. Dai, Y. Guo, X. Zhao, Y. Wang, Z. Wang, W. Han, and L. Chen, "Effective and persistent antitumor activity of HER2-directed CAR-T cells against gastric cancer cells in vitro and xenotransplanted tumors in vivo," *Protein Cell* **9**, 867–878 (2018).
- ³²A. Szoor, G. Toth, B. Zsebik, V. Szabo, Z. Eshhar, H. Abken, and G. Vereb, "Trastuzumab derived HER2-specific CARs for the treatment of trastuzumab-resistant breast cancer: CAR T cells penetrate and eradicate tumors that are not accessible to antibodies," *Cancer Lett.* **484**, 1–8 (2020).
- ³³S. Herter, L. Morra, R. Schlenker, J. Sulcova, L. Fahrni, I. Waldhauer, S. Lehmann, T. Reisländer, I. Agarkova, J. M. Kelm, C. Klein, P. Umama, and M. Bacac, "A novel three-dimensional heterotypic spheroid model for the assessment of the activity of cancer immunotherapy agents," *Cancer Immunol. Immunother.* **66**, 129–140 (2017).
- ³⁴Z. Chen, S. Han, A. Sanny, D. L. Chan, D. van Noort, W. Lim, A. H. Tan, and S. Park, "3D hanging spheroid plate for high-throughput CAR T cell cytotoxicity assay," *J. Nanobiotechnol.* **20**, 30 (2022).
- ³⁵G. Mehta, A. Y. Hsiao, M. Ingram, G. D. Luker, and S. Takayama, "Opportunities and challenges for use of tumor spheroids as models to test drug delivery and efficacy," *J. Control Release* **164**, 192–204 (2012).
- ³⁶S. El Harane, B. Zidi, N. El Harane, K. H. Krause, T. Matthes, and O. Preynat-Seauve, "Cancer spheroids and organoids as novel tools for research and therapy: State of the art and challenges to guide precision medicine," *Cells* **12**, 192 (2023).
- ³⁷A. Pavesi, A. T. Tan, S. Koh, A. Chia, M. Colombo, E. Antonicchia, C. Miccolis, E. Ceccarello, G. Adriani, M. T. Raimondi, R. D. Kamm, and A. Bertoletti, "A 3D microfluidic model for preclinical evaluation of TCR-engineered T cells against solid tumors," *JCI Insight* **2**, e89762 (2017).
- ³⁸Z. Wan, M. A. Floryan, M. F. Coughlin, S. Zhang, A. X. Zhong, S. E. Shelton, X. Wang, C. Xu, D. A. Barbie, and R. D. Kamm, "New strategy for promoting vascularization in tumor spheroids in a microfluidic assay," *Adv. Healthcare Mater.* **12**, e2201784 (2023).
- ³⁹K. Paterson, S. Paterson, T. Mulholland, S. B. Coffelt, and M. Zagnoni, "Assessment of CAR-T cell-mediated cytotoxicity in 3D microfluidic cancer co-culture models for combination therapy," *IEEE Open J. Eng. Med. Biol.* **3**, 86–95 (2022).
- ⁴⁰E. Ruffo, A. A. Butchy, Y. Tivon, V. So, M. Kvorjak, A. Parikh, E. L. Adams, N. Miskov-Zivanov, O. J. Finn, A. Deiters, and J. Lohmueller, "Post-translational covalent assembly of CAR and synNotch receptors for programmable antigen targeting," *Nat. Commun.* **14**, 2463 (2023).
- ⁴¹J. H. Cho, J. J. Collins, and W. W. Wong, "Universal chimeric antigen receptors for multiplexed and logical control of T cell responses," *Cell* **173**, 1426–1438 e1411 (2018).
- ⁴²K. Kudo, C. Imai, P. Lorenzini, T. Kamiya, K. Kono, A. M. Davidoff, W. J. Chng, and D. Campana, "T lymphocytes expressing a CD16 signaling receptor exert antibody-dependent cancer cell killing," *Cancer Res.* **74**, 93–103 (2014).
- ⁴³J. Lohmueller, J. D. Ham, M. Kvorjak, and O. J. Finn, "mSA2 affinity-enhanced biotin-binding CAR T cells for universal tumor targeting," *Oncoimmunology* **7**, e1368604 (2017).
- ⁴⁴J. S. Y. Ma, J. Y. Kim, S. A. Kazane, S. H. Choi, H. Y. Yun, M. S. Kim, D. T. Rodgers, H. M. Pugh, O. Singer, S. B. Sun, B. R. Fonslow, J. N. Kochenderfer, T. M. Wright, P. G. Schultz, T. S. Young, C. H. Kim, and Y. Cao, "Versatile

- strategy for controlling the specificity and activity of engineered T cells," *Proc. Natl. Acad. Sci. U. S. A.* **113**, E450–E458 (2016).
- ⁴⁵K. Tamada, D. Geng, Y. Sakoda, N. Bansal, R. Srivastava, Z. Li, and E. Davila, "Redirecting gene-modified T cells toward various cancer types using tagged antibodies," *Clin. Cancer Res.* **18**, 6436–6445 (2012).
- ⁴⁶D. T. Rodgers, M. Mazagova, E. N. Hampton, Y. Cao, N. S. Ramadoss, I. R. Hardy, A. Schulman, J. Du, F. Wang, O. Singer, J. Ma, V. Nunez, J. Shen, A. K. Woods, T. M. Wright, P. G. Schultz, C. H. Kim, and T. S. Young, "Switch-mediated activation and retargeting of CAR-T cells for B-cell malignancies," *Proc. Natl. Acad. Sci. U. S. A.* **113**, E459–E468 (2016).
- ⁴⁷K. Urbanska, E. Lanitis, M. Poussin, R. C. Lynn, B. P. Gavin, S. Kelderman, J. Yu, N. Scholler, and D. J. Powell, Jr., "A universal strategy for adoptive immunotherapy of cancer through use of a novel T-cell antigen receptor," *Cancer Res.* **72**, 1844–1852 (2012).
- ⁴⁸M. Bachmann, "The UniCAR system: A modular CAR T cell approach to improve the safety of CAR T cells," *Immunol. Lett.* **211**, 13–22 (2019).
- ⁴⁹N. G. Minutolo, E. E. Hollander, and D. J. Powell, Jr., "The emergence of universal immune receptor T cell therapy for cancer," *Front. Oncol.* **9**, 176 (2019).
- ⁵⁰M. Hamieh, J. Mansilla-Soto, I. Riviere, and M. Sadelain, "Programming CAR T cell tumor recognition: tuned antigen sensing and logic gating," *Cancer Discovery* **13**, 829–843 (2023).
- ⁵¹J. H. Choe, P. B. Watchmaker, M. S. Simic, R. D. Gilbert, A. W. Li, N. A. Krasnow, K. M. Downey, W. Yu, D. A. Carrera, A. Celli, J. Cho, J. D. Briones, J. M. Duecker, Y. E. Goretzky, R. Dannenfelser, L. Cardarelli, O. Troyanskaya, S. S. Sidhu, K. T. Roybal, H. Okada, and W. A. Lim, "SynNotch-CAR T cells overcome challenges of specificity, heterogeneity, and persistence in treating glioblastoma," *Sci. Transl. Med.* **13**, eabe7378 (2021).
- ⁵²D. J. Slamon, B. Leyland-Jones, S. Shak, H. Fuchs, V. Paton, A. Bajamonde, T. Fleming, W. Eiermann, J. Wolter, M. Pegram, J. Baselga, and L. Norton, "Use of chemotherapy plus a monoclonal antibody against HER2 for metastatic breast cancer that overexpresses HER2," *N. Engl. J. Med.* **344**, 783–792 (2001).
- ⁵³D. G. Song, Q. Ye, M. Poussin, J. A. Chacon, M. Figini, and D. J. Powell, Jr., "Effective adoptive immunotherapy of triple-negative breast cancer by folate receptor-alpha redirected CAR T cells is influenced by surface antigen expression level," *J. Hematol. Oncol.* **9**, 56 (2016).
- ⁵⁴K. N. Moore, A. Angelergues, G. E. Konecny, Y. Garcia, S. Banerjee, D. Lorusso, J. Y. Lee, J. W. Moroney, N. Colombo, A. Roszak, J. Tromp, T. Myers, J. W. Lee, M. Beiner, C. M. Cosgrove, D. Cibula, L. P. Martin, R. Sabatier, J. Buscema, P. Estevez-Garcia, L. Coffman, S. Nicum, L. R. Duska, S. Pignata, F. Galvez, Y. Wang, M. Method, A. Berkenblit, D. Bello Roufai, and T. Van Gorp, Gynecologic Oncology Group Partners and the European Network of Gynaecological Oncological Trial Groups, "Mirvetuximab soravtansine in FRZ-positive, platinum-resistant ovarian cancer," *N. Engl. J. Med.* **389**, 2162–2174 (2023).
- ⁵⁵L. Gattinoni, C. A. Klebanoff, D. C. Palmer, C. Wrzesinski, K. Kerstann, Z. Yu, S. E. Finkelstein, M. R. Theoret, S. A. Rosenberg, and N. P. Restifo, "Acquisition of full effector function in vitro paradoxically impairs the in vivo antitumor efficacy of adoptively transferred CD8⁺ T cells," *J. Clin. Invest.* **115**, 1616–1626 (2005).
- ⁵⁶B. Pinto, A. C. Henriques, P. M. A. Silva, and H. Bousbaa, "Three-dimensional spheroids as in vitro preclinical models for cancer research," *Pharmaceutics* **12**, 1186 (2020).
- ⁵⁷J. Friedrich, C. Seidel, R. Ebner, and L. A. Kunz-Schughart, "Spheroid-based drug screen: Considerations and practical approach," *Nat. Protoc.* **4**, 309–324 (2009).
- ⁵⁸S. Raghavan, P. Mehta, Y. Xie, Y. L. Lei, and G. Mehta, "Ovarian cancer stem cells and macrophages reciprocally interact through the WNT pathway to promote pro-tumoral and malignant phenotypes in 3D engineered microenvironments," *J. Immunother. Cancer* **7**, 190 (2019).
- ⁵⁹K. Fischer, P. Hoffmann, S. Voelkl, N. Meidenbauer, J. Ammer, M. Edinger, E. Gottfried, S. Schwarz, G. Rothe, S. Hoves, K. Renner, B. Timischl, A. Mackensen, L. Kunz-Schughart, R. Andreesen, S. W. Krause, and M. Kreutz, "Inhibitory effect of tumor cell-derived lactic acid on human T cells," *Blood* **109**, 3812–3819 (2007).
- ⁶⁰N. Gupta, J. R. Liu, B. Patel, D. E. Solomon, B. Vaidya, and V. Gupta, "Microfluidics-based 3D cell culture models: Utility in novel drug discovery and delivery research," *Bioeng. Transl. Med.* **1**, 63–81 (2016).
- ⁶¹G. Ronteix, S. Jain, C. Angely, M. Cazaux, R. Khazen, P. Bousso, and C. N. Baroud, "High resolution microfluidic assay and probabilistic modeling reveal cooperation between T cells in tumor killing," *Nat. Commun.* **13**, 3111 (2022).
- ⁶²M. S. Y. Lam, J. A. Reales-Calderon, J. R. Ow, J. J. Y. Aw, D. Tan, R. Vijayakumar, E. Ceccarello, T. Tabaglio, Y. T. Lim, W. L. Chien, F. Lai, A. T. Tanoto, Q. Chen, R. M. Sobota, G. Adriani, A. Bertoletti, E. Guccione, and A. Pavesi, "G9a/GLP inhibition during ex vivo lymphocyte expansion increases in vivo cytotoxicity of engineered T cells against hepatocellular carcinoma," *Nat. Commun.* **14**, 563 (2023).
- ⁶³R. Alonso-Matilla, P. P. Provenzano, and D. J. Odde, "Optimal cell traction forces in a generalized motor-clutch model," *Biophys. J.* **122**, 3369–3385 (2023).
- ⁶⁴L. S. Prah and D. J. Odde, "Modeling cell migration mechanics," *Adv. Exp. Med. Biol.* **1092**, 159–187 (2018).
- ⁶⁵Y. Ando, E. L. Siegler, H. P. Ta, G. E. Cinay, H. Zhou, K. A. Gorrell, H. Au, B. M. Jarvis, P. Wang, and K. Shen, "Evaluating CAR-T cell therapy in a hypoxic 3D tumor model," *Adv. Healthcare Mater.* **8**, e1900001 (2019).
- ⁶⁶L. Nagy, M. Mezosi-Csaplár, I. Rebenku, G. Vereb, and A. Szöör, "Universal CAR T cells targeted to HER2 with a biotin-trastuzumab soluble linker penetrate spheroids and large tumor xenografts that are inherently resistant to trastuzumab mediated ADCC," *Front. Immunol.* **15**, 1365172 (2024).
- ⁶⁷R. C. Sterner and R. M. Sterner, "CAR-T cell therapy: Current limitations and potential strategies," *Blood Cancer J.* **11**, 69 (2021).
- ⁶⁸T. Yan, L. Zhu, and J. Chen, "Current advances and challenges in CAR T-Cell therapy for solid tumors: Tumor-associated antigens and the tumor microenvironment," *Exp. Hematol. Oncol.* **12**, 14 (2023).
- ⁶⁹S. Budhu, J. D. Loike, A. Pandolfi, S. Han, G. Catalano, A. Constantinescu, R. Clynes, and S. C. Silverstein, "CD8⁺ T cell concentration determines their efficiency in killing cognate antigen-expressing syngeneic mammalian cells in vitro and in mouse tissues," *J. Exp. Med.* **207**, 223–235 (2010).
- ⁷⁰Q. Mu, M. Jiang, Y. Zhang, F. Wu, H. Li, W. Zhang, F. Wang, J. Liu, L. Li, D. Wang, W. Wang, S. Li, H. Song, and D. Tang, "Metformin inhibits proliferation and cytotoxicity and induces apoptosis via AMPK pathway in CD19-chimeric antigen receptor-modified T cells," *Oncotargets Ther.* **11**, 1767–1776 (2018).
- ⁷¹S. Halle, K. A. Keyser, F. R. Stahl, A. Busche, A. Marquardt, X. Zheng, M. Galla, V. Heissmeyer, K. Heller, J. Boelter, K. Wagner, Y. Bischoff, R. Martens, A. Braun, K. Werth, A. Uvarovskii, H. Kempf, M. Meyer-Hermann, R. Arens, M. Kremer, G. Sutter, M. Messerle, and R. Forster, "In vivo killing capacity of cytotoxic T cells is limited and involves dynamic interactions and T cell cooperativity," *Immunity* **44**, 233–245 (2016).
- ⁷²Y. Masugi, T. Abe, A. Ueno, Y. Fujii-Nishimura, H. Ojima, Y. Endo, Y. Fujita, M. Kitago, M. Shinoda, Y. Kitagawa, and M. Sakamoto, "Characterization of spatial distribution of tumor-infiltrating CD8⁺ T cells refines their prognostic utility for pancreatic cancer survival," *Mod. Pathol.* **32**, 1495–1507 (2019).
- ⁷³J. L. Carstens, P. Correa de Sampaio, D. Yang, S. Barua, H. Wang, A. Rao, J. P. Allison, V. S. LeBleu, and R. Kalluri, "Spatial computation of intratumoral T cells correlates with survival of patients with pancreatic cancer," *Nat. Commun.* **8**, 15095 (2017).
- ⁷⁴B. O. Tschumi, N. Dumauthioz, B. Marti, L. Zhang, E. Lanitis, M. Irving, P. Schneider, J. P. Mach, G. Coukos, P. Romero, and A. Donda, "CAR T cells are prone to Fas- and DR5-mediated cell death," *J. Immunother. Cancer* **6**, 71 (2018).
- ⁷⁵M. D. Poskus, T. Wang, Y. Deng, S. Borchering, J. Atkinson, and I. K. Zervantonakis, "Fabrication of 3D-printed molds for polydimethylsiloxane-based microfluidic devices using a liquid crystal display-based vat photopolymerization process: Printing quality, drug response and 3D invasion cell culture assays," *Microsyst. Nanoeng.* **9**, 140 (2023).
- ⁷⁶B. E. Welm, G. J. Dijkgraaf, A. S. Bledau, A. L. Welm, and Z. Werb, "Lentiviral transduction of mammary stem cells for analysis of gene function during development and cancer," *Cell Stem Cell* **2**, 90–102 (2008).